Hindawi Publishing Corporation
Advances in Optical Technologies
Volume 2008, Article ID 532368, 10 pages
doi:10.1155/2008/532368

Research Article

A Ratiometric Fluorescence Imaging System for Surgical Guidance

Eduardo H. Moriyama,[1,2] Anthony Kim,[1] Arjen Bogaards,[1] Lothar Lilge,[1] and Brian C. Wilson[1]

[1] *Division of Biophysics and Bioimaging, Ontario Cancer Institute, University Health Network, 610 University Avenue 7-420, Toronto, ON, Canada M5G 2M9*
[2] *Department of Physics, Ryerson University, 350 Victoria Street, Toronto, ON, Canada M5B 2K3*

Correspondence should be addressed to Brian C. Wilson, wilson@uhnres.utoronto.ca

Received 3 March 2008; Accepted 28 June 2008

Recommended by Stoyan Tanev

A 3-chip CCD imaging system has been developed for quantitative in vivo fluorescence imaging. This incorporates a ratiometric algorithm to correct for the effects of tissue optical absorption and scattering, imaging "geometry" and tissue autofluorescence background. The performance was characterized, and the algorithm was validated in tissue-simulating optical phantoms for quantitative measurement of the fluorescent molecule protoporphyrin IX (PpIX). The technical feasibility to use this system for fluorescence-guided surgical resection of malignant brain tumor tissue was assessed in an animal model in which PpIX was induced exogenously in the tumor cells by systemic administration of aminolevulinic acid (ALA).

Copyright © 2008 Eduardo H. Moriyama et al. This is an open access article distributed under the Creative Commons Attribution License, which permits unrestricted use, distribution, and reproduction in any medium, provided the original work is properly cited.

1. INTRODUCTION

Intracranial brain tumors are the most common and aggressive primary tumors in the central nervous system (CNS) and carry one of the worst prognosis of all types of cancers. Advances in surgery, radiotherapy, and chemotherapy have resulted in only modest improvement in patient survival [1]. Radical surgical resection is considered the standard procedure for treatment of high-grade gliomas, and maximizing the degree of tumor resection has been related to improvement of patient survival [2, 3]. However, due to the infiltrative nature of most of the gliomas, complete resection is difficult to achieve, resulting in high risk of tumor recurrence [2]. Hence, more sensitive and specific techniques are needed to aid in the identification of malignant tissue intraoperatively and, thereby, to increase the completeness of tumor resection without damaging adjacent critical normal brain structures and function [4]. Such techniques include magnetic resonance imaging (MRI) [5, 6], ultrasound [7], and optical technologies [8–10].

Fluorescence imaging is particularly promising to identify malignant tissues *in vivo*, exploiting either intrinsic fluorescence characteristics (autofluorescence) [11–13] or the preferential accumulation or targeting of administered (exogenous) fluorophores [14–16]. Fluorescent agents such as fluorescein [17] and porphyrins [8, 18, 19] are suitable agents for detection of neoplastic cells during intraoperative tumor removal, on account of their preferential accumulation and/or retention in malignant tissues. Recently, the main effort has been on fluorescence-guided resection (FGR) of brain tumors using protoporphyrin IX (PpIX), which is preferentially synthesized in brain tumor cells relative to normal brain following administration of aminolevulinic acid (ALA). This approach has demonstrated more complete resection of brain tumors compared to surgery under white light alone, in both preclinical animal models [20, 21] and in patients [18, 22]. However, making FGR using exogenous fluorophores, including ALA-PpIX, a quantitative and hence, objective and reproducible technique is challenging, due the effects of multiple scattering and absorption of the excitation and emission light and the background of tissue autofluorescence. To date, only semiquantitative information on the concentration and distribution of fluorescent probes *in vivo* [23–25] has been possible.

Several approaches have been investigated for quantitative fluorescence measurements *in vivo*, including tomographic imaging [26, 27], fluorescence lifetime imaging [28], fiberoptic point fluorescence spectroscopies [29, 30], and

ratiometric correction methods [31–33]. Here, we will focus on the last of these, in which the objective is to make multiple spectral measurements that are then combined through an empirical or biophysical model to correct for the tissue attenuation and/or autofluorescence effects. As we will demonstrate, the advantage is that this can be implemented in real-time imaging mode, which is clinically desirable. In the simplest approach, correction is performed using single excitation and emission wavelengths [34, 35], but this does not correct for tissue autofluorescence [36]. As we recently showed in a modeling study [37], the use of multiple excitation and/or emission wavelengths can virtually eliminate the tissue autofluorescence and also enable quantitative measurements of fluorophores [36–40], such that the fluorescent signal depends only on the concentration of the fluorophore. This has been validated in phantoms for a wide range of fluorophore concentrations (in the case of PpIX, e.g., to $<0.1\,\mu g\,mL^{-1}$) and tissue optical properties [41].

Here, we present a prototype FGR instrument that provides video-rate digital fluorescence imaging incorporating a double-ratiometric correction method that is optimized for intraoperative identification of brain tumors. Validation studies in phantoms are presented to demonstrate the performance of the system, and preliminary experiments are presented in resection of intracranial brain tumor in a rat model *in vivo* to illustrate its practicality and functionality.

2. MATERIALS AND METHODS

2.1. System description

The fluorescence imaging system was designed primarily for surgical guidance and is shown in Figure 1. The light source comprises a 300 W xenon lamp (Cermax, Perkin Elmer, CA, USA) focused through a filter wheel into a 5 mm diameter liquid light guide (Model 495 FR, Karl Storz, Tuttlingen, Germany) that is coupled into a 10 mm diameter rigid clinical laparoscope (Model 871 1AA, Karl Storz, Tuttlingen Germany). The collection component of the imaging system is based on a 3-CCD compact camera (DXC-C33, Sony, ON, Canada) operating at 30 frames s^{-1}(NTSC) with 796×494 pixels and 8-bit dynamic range. A long-pass 500 nm filter (Custom made, Chroma Technologies, VT, USA) is placed between the camera and the laparoscope. This filter deliberately leaks a small fraction ($\sim 10^{-4}$) of the UV/blue excitation light to allow measurement of the diffuse reflectance signal from the tissue for the ratiometric algorithm described below. Spectral response curves for the red, green, and blue channels of the CCD were measured using a standard color target (ColorChecker Chart: Gretag Macbeth, Grand Rapids, MI, USA) illuminated by a tungsten-halogen light source (LS-1: Ocean Optics, Dunedin, FL, USA). For this, the images of the color target were taken through the laparoscope without the fluorescence emission filter installed. Serial filters spanning from 420 to 750 nm were placed in front of the laparoscope lens for each of the color target images. The spectral response of the camera-laparoscope optical chain

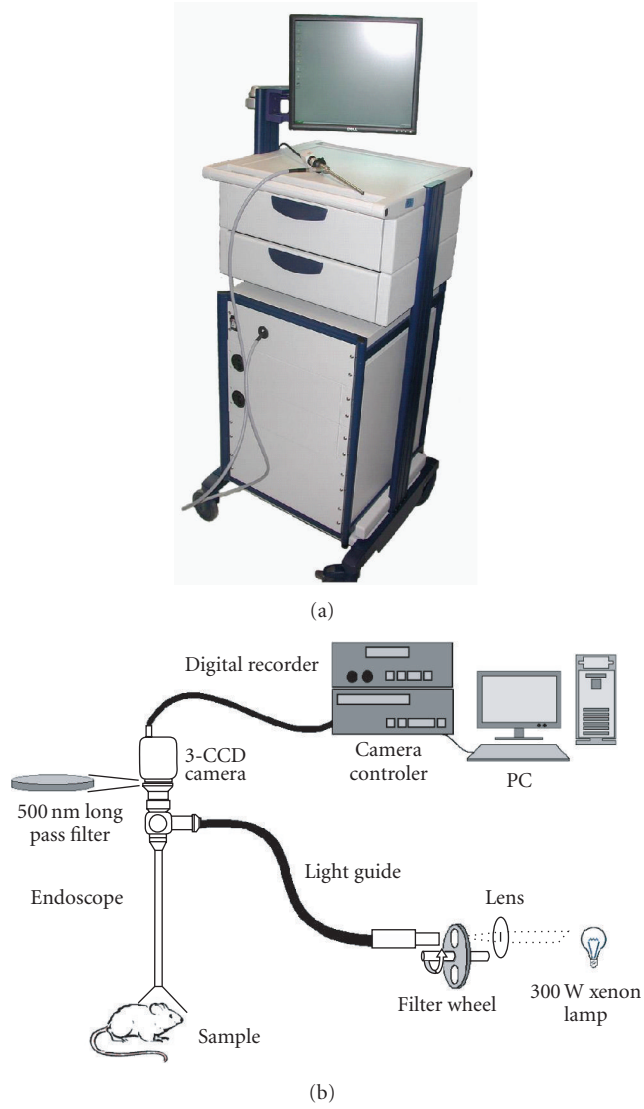

Figure 1: (a) Photograph and (b) schematic of the system.

was determined and averaged from 4 spectrally-neutral shades.

The fluorescence imaging system features a dual-excitation capability. The filter wheel holds two different excitation filters, and its rotation rate is such that consecutive camera frames are excited by alternating excitation wavelengths. For the present study, the excitation filters had central wavelengths, λ_{ex1}, at the PpIX Soret maxima of 405 nm (full width at half maximum, FWHM = 96 nm) and at 440 nm (FWHM = 60 nm). The latter was chosen as the shortest wavelength lying above the main PpIX Soret band in order to allow for correction for the tissue autofluorescence. It is assumed then that the tissue optical properties are comparable at these two wavelengths, since they are not too far apart. Both wavelengths can induce high levels of autofluorescence in tumor and normal tissues. The delivered power at each wavelength was approximately 50 mW cm^{-2} at a typical working distance of 2 cm from

Table 1: Optical properties of the liquid phantoms at 635 nm.

	Reduced scattering coefficient μ_s' (cm^{-1})	Absorption coefficient μ_a (cm^{-1})
Phantom A	7	1.6
Phantom B	7	3.2
Phantom C	14	1.6
Phantom D	14	3.2

the tissue surface. The digital video output is captured by a laptop computer and can be displayed for visualization of the processed fluorescence images in real time. The image processing software (Hytek Automation, Waterloo, ON, Canada) was based on LabVIEW (National Instruments Corp., Austin, TX, USA) and could execute multiplication, division, addition, or subtraction on each channel.

2.2. System characterization

The spatial resolution of the imaging system was determined using a standard 1951 USAF glass slide resolution target (Edmund Optics, NJ, USA) placed 2 cm from the front end of the laparoscope, resulting in a field of view of 12.7×8.2 mm. To characterize the system performance for fluorescence imaging, tissue-simulating liquid phantoms were prepared, comprising PpIX (Sigma-Aldrich, ON, Canada) dissolved in 1 mM dimethyl sulfoxide (DMSO) with methylene blue dye added as the optical absorber and the lipoprotein emulsion Intralipid (Fresenius Kabi, *Uppsala*, Sweden) to provide optical scattering [42]. The corresponding absorption and reduced scattering coefficients are given in Table 1, based on well-established literature values. The system sensitivity was measured using varying PpIX concentrations: 2.5, 1.25, 0.62, 0.31, 0.15, 0.075, and 0.039 μg mL^{-1}. At each concentration, fluorescence images were taken at both excitation wavelengths at distances of 2, 3, 4, or 5 cm from the phantom surface, with the camera focused at the 2 cm working distance. The signal in the red channel of the 3-CCD was plotted as a function of PpIX concentration. The fluorescence signal was collected at 0°, 15°, or 30° from the vertical axis to determine the influence of the imaging geometry.

The ratiometric method applied here was developed by our group previously and is based on using 2 excitation and 2 emission wavelengths [41]. The first excitation wavelength is in the absorption peak of PpIX ($\lambda_{ex1} = 405$ nm) and, for each image pixel, the emitted red fluorescence (560–750 nm) is divided by the signal from the diffusely reflected excitation light. Next, this fluorescence/reflectance ratio is divided by the same ratio calculated using the second-excitation wavelength ($\lambda_{ex2} = 440$ nm). Thus, the signal, Q, in each pixel is given by

$$Q = \frac{F(\lambda_{ex1}, \lambda_{em1})}{R(\lambda_{ex1})} \times \frac{R(\lambda_{ex2})}{F(\lambda_{ex2}, \lambda_{em1})}. \quad (1)$$

2.3. In vivo tests

To test the feasibility and functionality of this imaging system and the double-ratio algorithm *in vivo*, PpIX fluorescence and diffuse reflectance images were acquired in an established rat brain tumor model [39] undergoing fluorescence-guided tumor resection. The rat glioma tumor model, CNS-1, was chosen as being highly infiltrative, a common characteristic of high-grade human gliomas that should present a valid test of the ability to detect residual tumor at the surgical margins. FGR was performed at 21 days following implantation of luciferase-transfected CNS-1^{luc} cells (3×10^5 cells, 2 mm below the dura, $n = 2$ per ALA dose) in the left brain hemisphere of Lewis rats (Charles River, MA, USA). PpIX was induced by administering aminolevulinic acid (ALA) in hydrochloride form (Sigma, Oakville, ON, Canada). This was dissolved in phosphate-buffered saline (20 mg mL^{-1}) with the pH adjusted to ~5.5 by 1N NaOH and then injected intraperitoneally (i.p.) at 20, 50, or 100 mg kg^{-1} at 2–4 hours before the surgical procedure/imaging. The animals were subdued by an i.p. mixture of ketamine and xylazine (80 and 13 mg kg^{-1}, resp.). A 2 cm incision was made in the scalp along the midline and held open by a retractor. A 1 cm craniotomy was performed using a burr drill, and the dura was carefully removed. To measure the uptake of PpIX in tumors, PpIX fluorescence spectra (450–750 nm) were acquired by means of a 400 μm fiberoptic probe, coupled to a spectrometer (Model S2000, Ocean Optics, FL, USA), placed in gentle contact with the tissue surface, and compared with PpIX fluorescence spectra from CNS-1^{luc} cell lysates measured using a spectrofluorimeter (SpectraMax M5; Molecular Devices, CA, USA) at 405 nm excitation after incubation with 1 mM ALA for 4 hours. FGR was performed by positioning the laparoscope tip at 2 cm above the surgical site. Tumor was identified by areas of evident red fluorescence and resected by means of suction through a glass tip with 0.5 mm inner diameter. Spectral images were acquired during tumor resection, which was terminated when red fluorescence was no longer detectable on the video monitor. The resected tissue was fixed in 10% formalin for sectioning H&E staining. Following resection, the presence of residual tumor cells was assessed semiquantitatively by applying 100 μL of 1 mM luciferin (Xenogen, Alameda, CA, USA) in PBS as the substrate for bioluminescence, which was observed *in vivo* using a commercial bioluminescence imaging system (IVIS, Xenogen). Immediately afterwards, the animals were sacrificed by intracardiac injection of 1 mg kg^{-1} of sodium pentobarbital (Euthanyl, MTC Pharmaceuticals, Cambridge, ON, Canada), and the whole brain was removed intact for sectioning and H&E staining for histopathological assessment.

3. RESULTS

3.1. System performance

Figure 2(a) shows the spectral response of the CCD camera in each of the 3 channels. The spatial modulation transfer function (MTF), measured using the resolution pattern at

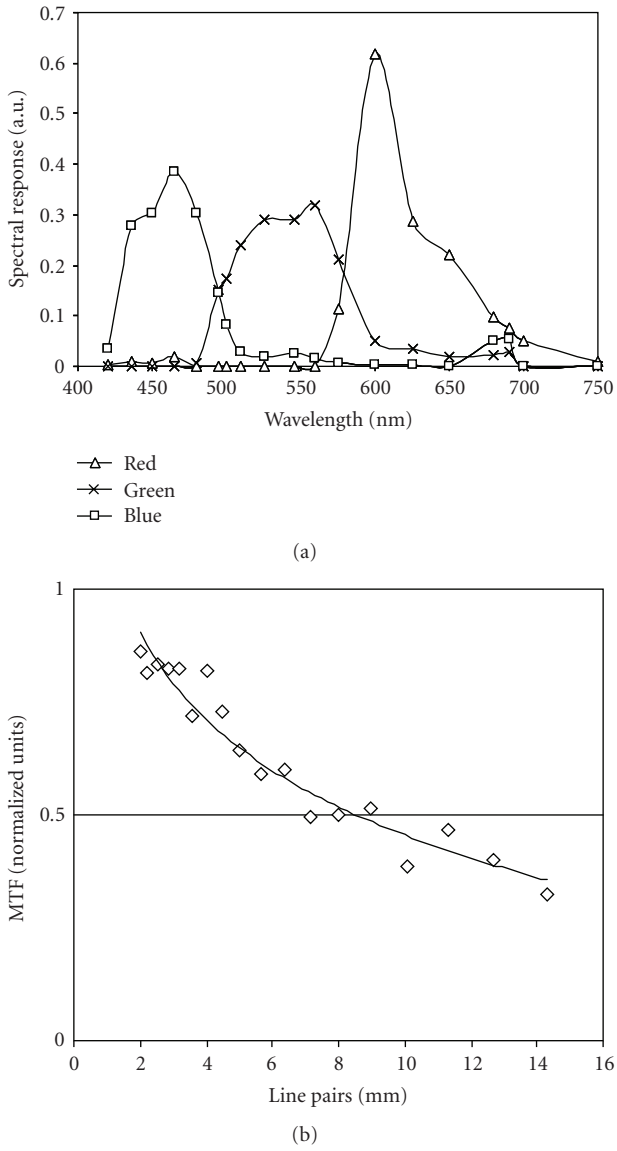

Figure 2: (a) Spectral response curves for the red, green, and blue channels of the 3-chip CCD, (b) fluorescence modulation transfer function measured at 2 cm working distance. The solid line is a logarithmic fit to the experimental data points.

a working distance of 2 cm from the laparoscope tip, is shown in Figure 2(b). The spatial resolution, defined at an MTF value of 50%, is 0.12 mm (8.5 line pairs per mm).

3.2. Efficacy of the ratiometric algorithm

The red-channel signal, corresponding to PpIX fluorescence, is plotted as a function of PpIX concentration for phantoms of different optical properties in Figure 3(a) and for different laparoscope-tissue distances in Figure 3(c). These demonstrate the strong dependence of the "raw" fluorescence signal on the tissue characteristics (due to attenuation of the excitation and fluorescent light) and imaging geometry, confirming the need to apply corrections to the data. Figures 3(b) and 3(d) show that the double-ratio method markedly reduces these differences, for example, at 2.5 μg mL^{-1} (i.e., the highest concentration used), the relative standard deviations of the fluorescence signal (i.e., stdev/mean $*$ 100%) are 26.1%, 13.1%, 28.2%, and 10.1% for Figures 3(a)–3(d), respectively. Figure 4 shows the corresponding data for varying angle between the laparoscope and the tissue surface.

3.3. Biological studies

In vitro and *in vivo* spectroscopic analysis of CNS-1 cells and tumors after administration of ALA for 4 hours (1 mM and 100 mg kg^{-1}, resp.) confirmed the presence of the PpIX fluorescence peak at 635 nm (see Figure 5(a)). Figures 5(b)–5(d) show examples that demonstrate the quality of the fluorescence images obtained with the system. Evident red fluorescence was observed from tumor areas at all ALA doses, demonstrating the capability to discriminate between tumor and normal brain tissues. The tumor-associated fluorescence increased from the lowest to the highest ALA dose, roughly proportionally. The normal brain showed no such trend. However, there was high variability in the fluorescence signals that was likely due in part to the small number of animals used in this feasibility study and in part to the intrinsic heterogeneity of the tumor model. The imaging system also detected diffuse and specular reflectance in the blue component, which aids in overall tissue orientation during surgery. No significant differences in PpIX fluorescence were found in normal brain tissues between the tumor-bearing and contralateral hemispheres (data not shown).

We also tested the system's ability to monitor fluorescence-guided resection of tumor. As illustrated by the example in Figure 6, it was possible in all animals to completely resect the visible fluorescing (tumor) tissue, as confirmed by histopathology (see Figure 7(c)). Despite this, bioluminescence imaging (see Figures 7(a)-7(b)) indicated the presence of small amounts of residual tumor, corresponding to ~100 cells at or close to the resection surface (as estimated from the bioluminescence signal).

4. DISCUSSION

The ability to accurately quantify fluorescence signals in optically-turbid media such as tissue is challenging, due to its complex dependence on many factors in addition to the fluorophore concentration, and in particular the tissue absorption and scattering properties, the measurement geometry and the background tissue autofluorescence. These issues have been discussed in many papers, as summarized by Bradley and Thorniley [36] and Bogaards et al. [41]. Several different fluorescence imaging systems have also been developed for *in vivo* applications, including the purpose of guiding tumor surgery and particularly in the brain. The intent in developing the present instrument was two-fold. Firstly, we wished to make a device that is compact and independent of any other surgical instrumentation. The approach implemented by Stummer and colleagues [18, 22, 43], for example, is to integrate fluorescence capabilities into an

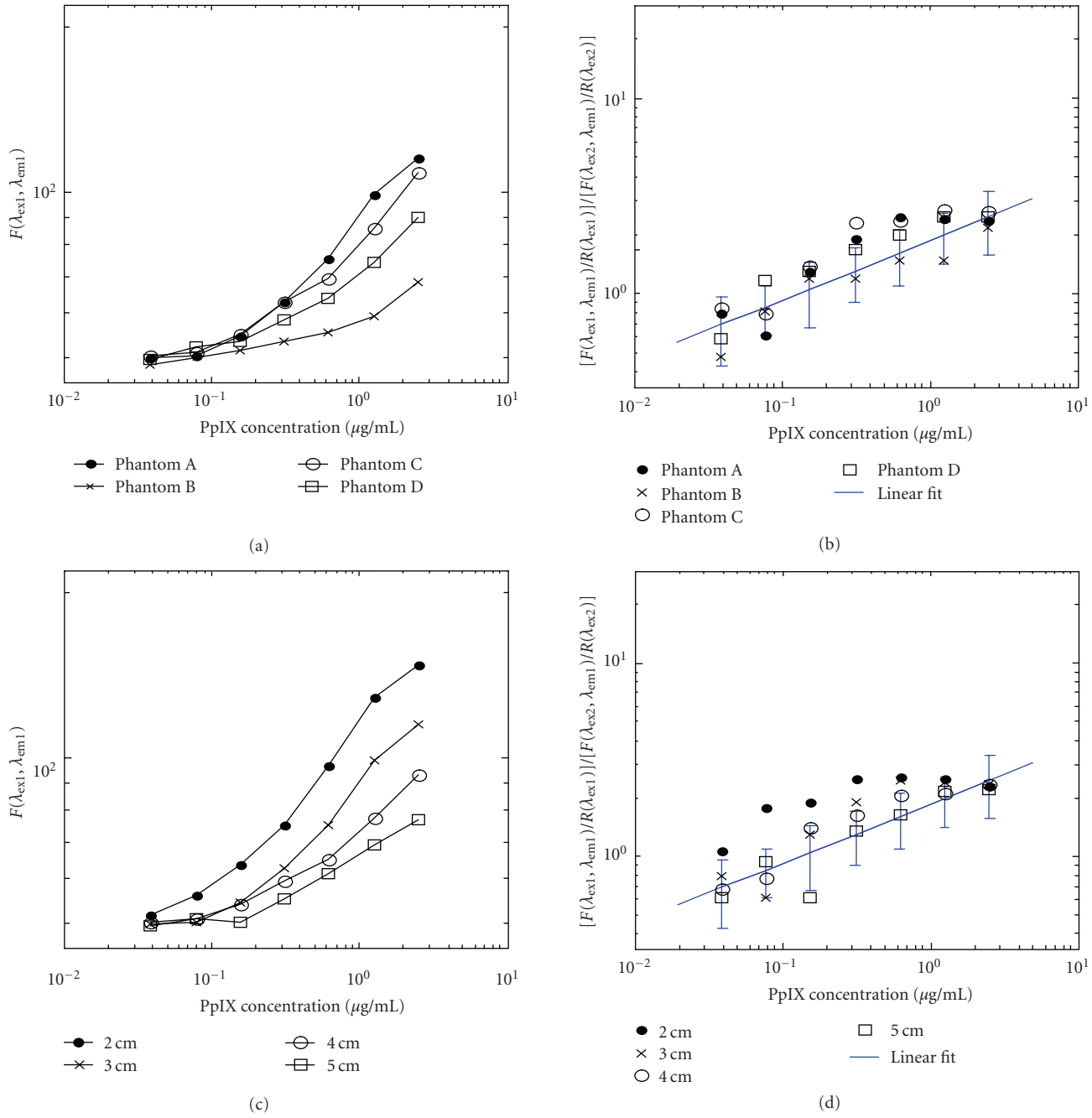

FIGURE 3: (a), (c) Relative PpIX fluorescence intensities as a function of PpIX concentration before and (b), (d) after application of the double-ratio algorithm, measured in the phantoms under different conditions. Linear regression fits to the combined data are shown in the corrected plots.

operating microscope. This certainly is a valid approach and has advantages in terms of ease of use, but limits its general surgical applicability. We intend in the near future to carry out a direct comparison of the performance of the present open-field device with the through-microscope technique. The second intent was to implement the double-wavelength ratiometric algorithm. While single-ratio correction has been used in other studies as a method to improve the information content in fluorescence-based diagnostics (e.g., $R_1 = F(\lambda_{ex1}, \lambda_{em1})/R(\lambda_{ex1})$, or $R_2 = F(\lambda_{ex2}, \lambda_{em2})/R(\lambda_{ex2})$) [32, 39, 44], the 2-excitation/2-detection wavelengths algorithm developed previously by our group [41] and implemented here appears to be particularly effective in minimizing the effects of tissue autofluorescence, geometric effects, and optical attenuation. The phantom studies presented above on the latter two factors confirm our previous modeling study of the efficacy of different correction algorithms [41]. In particular, including the reflectance signal (by allowing

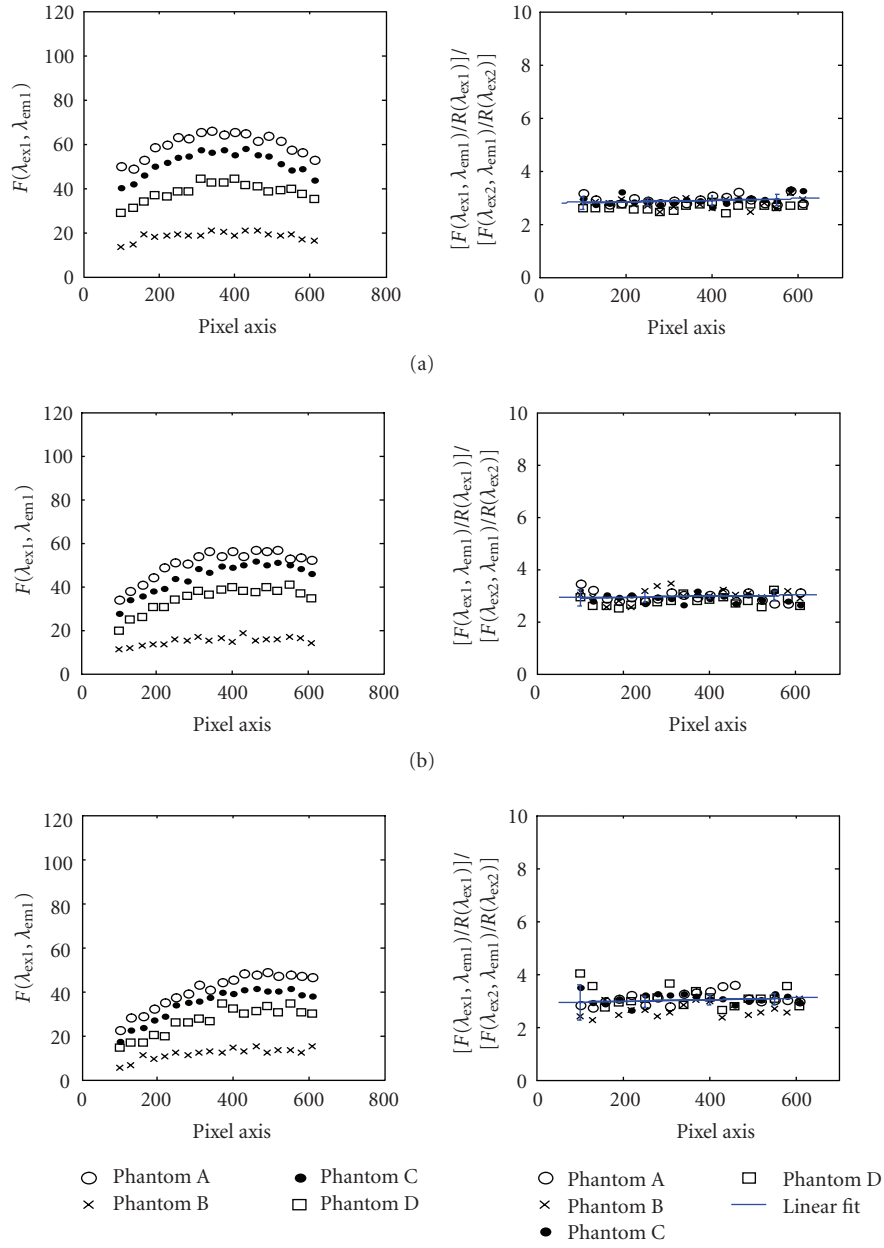

Figure 4: Relative PpIX fluorescence intensities as a function on position on the CCD image (centered at the 400 pixel value), showing how this varies with the angle between the optical axis (i.e., laparoscope direction) and the tissue surface, for the different optical properties: (a) 0°, (b) 15°, (c) 30°. Graphs on the left are the uncorrected data; those on the right are after applying the double-ratio algorithm (with linear fits to the combined data). In each plot, the signals are summed along the axis perpendicular to the x-axis of the graphs on the 3D CCD array. All measurements were made at 2 cm working distance.

a small fraction of the excitation light to leak through the excitation filter) minimizes the dependence on variations in autofluorescence. As shown by the phantom studies (see Figures 3 and 4), the algorithm also largely removes the dependence on the tissue optical properties and imaging geometry, since the effects of these factors are similar at the 2 excitation wavelengths, so that they are largely cancelled by taking the ratio of the signals at these wavelengths, which aids in applying an objective and quantitative criterion (e.g., a threshold concentration) to differentiate between diseased and non-diseased tissues. This overcomes a significant weakness of previous studies, including clinical trials, in which only subjective and qualitative criteria were applied [45].

The principal advantage of using a 3-chip CCD camera in this device is that the red, green, and blue components can

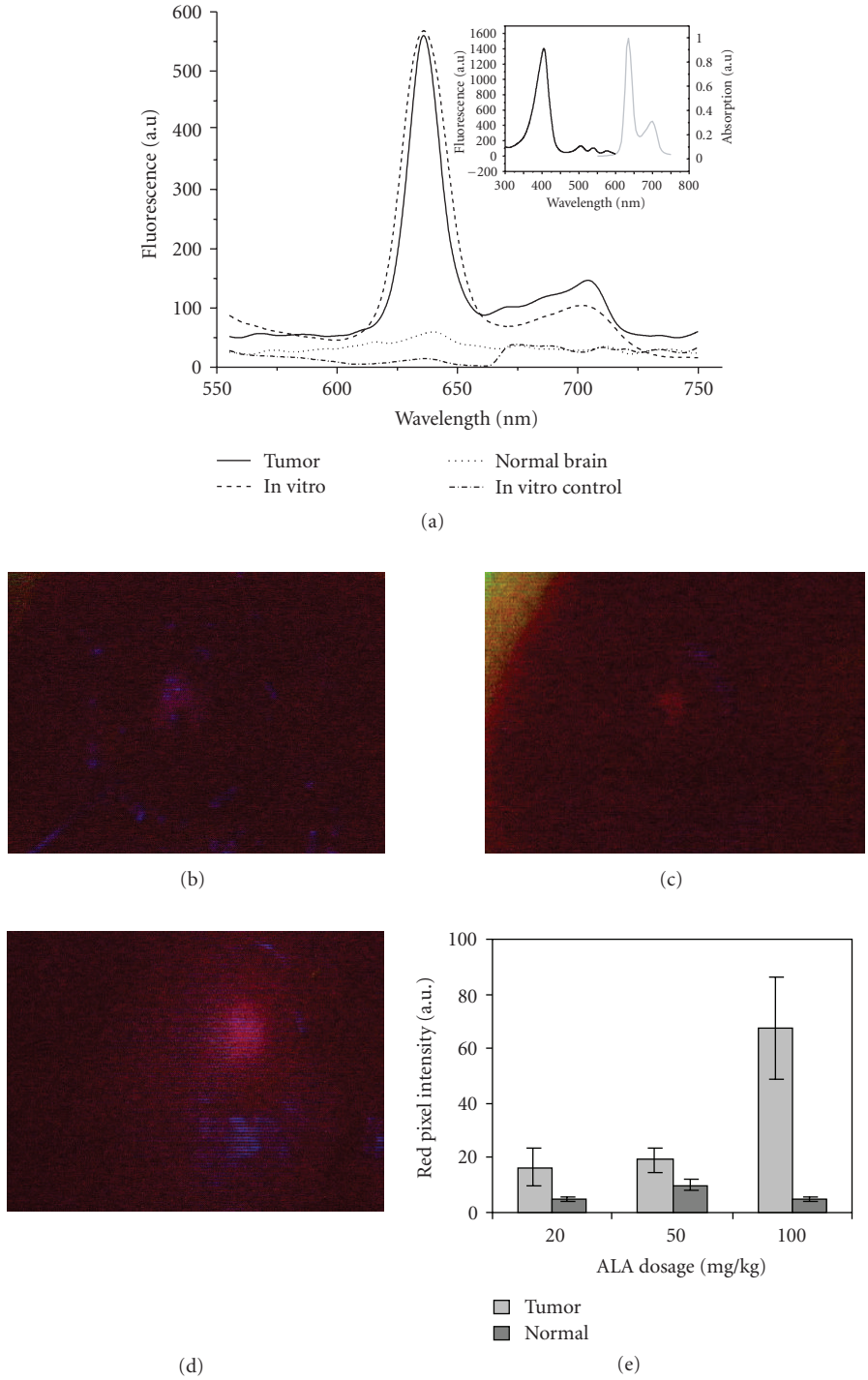

Figure 5: (a) Normalized PpIX fluorescence spectra of tumor and normal contralateral brain *in vivo*, 4 hours after i.p. administration of 100 mg kg^{-1} of ALA, and corresponding spectra in CNS-1 cells *in vitro* compared to controls (no ALA). The insert shows the excitation and emission spectra of PpIX in solution. (b)–(d) *In vivo* fluorescence images of PpIX in tumor after i.p. injection of 20, 50, and 100 mg kg^{-1} ALA, respectively. (e) PpIX fluorescence from tumor-bearing animals 4 hours after injection of different ALA doses in tumor and contralateral normal brain (means ±1 standard deviation: $N = 2$).

be independently augmented or attenuated in the resulting image, depending on the spectral band that exhibits the highest contrast between tumor and normal tissue. Custom software integrates the dual excitation and RGB components into a real-time (video rate) composite that can be tailored to enhance a large number of different fluorophores.

The spectral images of PpIX in phantoms and *in vivo* demonstrated excellent spatial resolution and contrast for

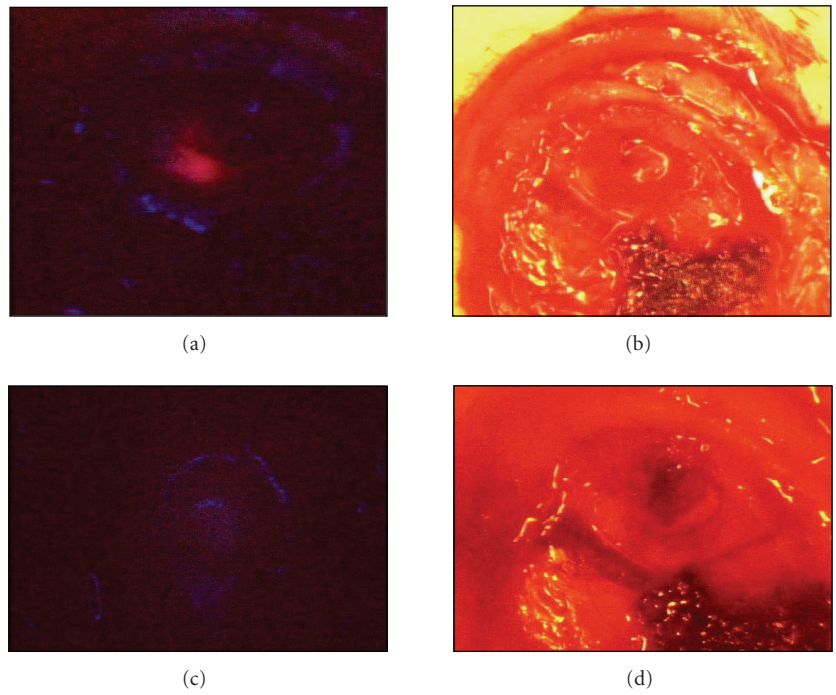

(a) (b) (c) (d)

Figure 6: (a), (c) Example of *in vivo* PpIX fluorescence (λ_{ex}: 405 nm) and (b), (d) white light images in the tumor resection cavity pre (a), (b) and post fluorescence-guided resection (c), (d). Surgery was performed 4 hours after ALA injection (100 mg kg^{-1}, i.p.). The blue areas represent specular reflection from the tissue surface.

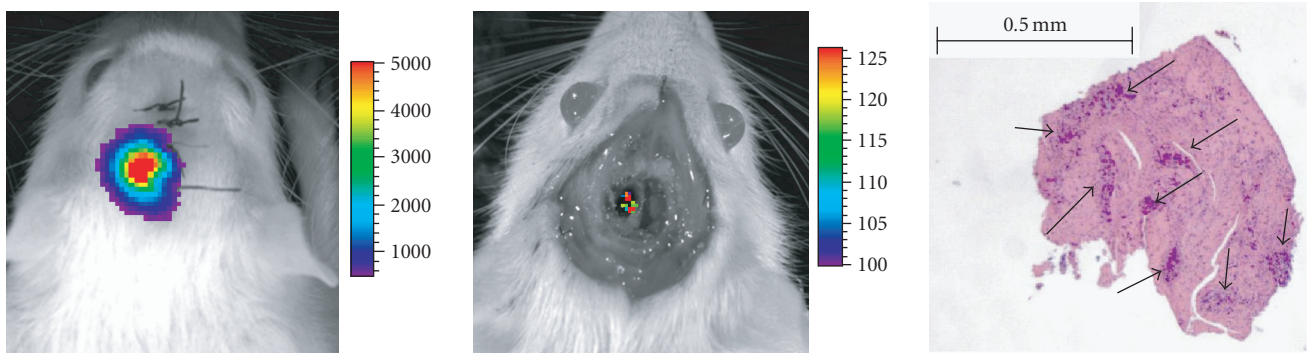

(a) (b) (c)

Figure 7: Example of *in vivo* bioluminescence imaging pre (a) and post (b) fluorescence-guided resection. The bioluminescence imaging of residual CNS-1^{luc} cells immediately after FGR corresponds to approximately 100 cells detected at the surface of the resection cavity. (c) H&E stained tissue section from the red-positive region in Figure 6(a). The arrows show nests of tumor cells.

visualization of residual tumors and the margins between normal and tumor tissues (see Figure 5). Hence, the technology should "extend the surgeon's eye" in the identification and localization of tumor tissue. In particular, the system should work better than simply imaging the uncorrected fluorescence signal, especially in areas of low fluorescence intensity, due to reduction of the dependence on tissue autofluorescence. Again, this will be evaluated by head-to-head comparisons in phantoms, animal models, and patients.

One of the most exciting possibilities for this method of ALA-PpIX fluorescence imaging for guiding brain tumor resection is to combine it with photodynamic therapy (PDT), and several groups, including our own, are pursuing this approach [20, 39]. The advantage of ALA-PpIX is that the same agent can serve both purposes, since PpIX is also well established as a PDT sensitizer. Further, since the PpIX is endogenously synthesized, we and others have shown its high selectivity for brain tumor relative to normal brain tissues, especially white matter [46–48].

As indicated in the Introduction, ALA-PpIX-based FGR has been shown to improve the completeness of glioma resection compared to standard white-light visualization [18–21]. However, the present study (see Figure 7), and

earlier work in a different brain tumor model [49] using bioluminescence post resection, show the likelihood of there being small amounts of residual tumor tissue that is below the fluorescence detection threshold. Hence, PDT applied intraoperatively immediately after resection should offer an additional level of tumor destruction and such combination studies are in progress, both preclinically [20, 42] and in human trials [50].

In conclusion, to date this instrument has met our objectives of a free-standing, easy-to-use, and highly sensitive intraoperative fluorescence imaging system for improved tumor resection. The phantom and previous modeling studies [41] have demonstrated the effectiveness of the double-ratio algorithm. Although limited in extent, the initial *in vivo* studies presented here have demonstrated the technical feasibility of the system to be used for fluorescence image-guided resection. Work is in progress in the CNS-1^{luc} brain tumor model using the system to optimize the ALA dose and the time interval between its administration and the resection to give the highest sensitivity and specificity. We have also confirmed the technical feasibility of the instrument in preliminary clinical tests in patients carried out during prostatectomy and in assessment of recurrent vulvar malignancy (data not shown). Systematic clinical tests are in progress or planned for a number of different tumor sites.

ACKNOWLEDGMENTS

This work was supported by NIH Grant PO1-CA43892 A. Kim was supported by NIH Grant RO1-NS052274. The authors thank Dr. Kai Zhang for his assistance with the imaging system and Mathieu Roy for preparing the phantoms.

REFERENCES

[1] F. G. Barker II, S. M. Chang, P. H. Gutin, et al., "Survival and functional status after resection of recurrent glioblastoma multiforme," *Neurosurgery*, vol. 42, no. 4, pp. 709–723, 1998.

[2] M. Lacroix, D. Abi-Said, D. R. Fourney, et al., "A multivariate analysis of 416 patients with glioblastoma multiforme: prognosis, extent of resection, and survival," *Journal of Neurosurgery*, vol. 95, no. 2, pp. 190–198, 2001.

[3] J. Yoshida, Y. Kajita, T. Wakabayashi, and K. Sugita, "Long-term follow-up results of 175 patients with malignant glioma: importance of radical tumour resection and postoperative adjuvant therapy with interferon, ACNU and radiation," *Acta Neurochirurgica*, vol. 127, no. 1-2, pp. 55–59, 1994.

[4] R. Zakhary, G. E. Keles, and M. S. Berger, "Intraoperative imaging techniques in the treatment of brain tumors," *Current Opinion in Oncology*, vol. 11, no. 3, pp. 152–156, 1999.

[5] M. J. McGirt, K. R. Bulsara, T. J. Cummings, et al., "Prognostic value of magnetic resonance imaging-guided stereotactic biopsy in the evaluation of recurrent malignant astrocytoma compared with a lesion due to radiation effect," *Journal of Neurosurgery*, vol. 98, no. 1, pp. 14–20, 2003.

[6] C. Nimsky, O. Ganslandt, M. Buchfelder, and R. Fahlbusch, "Intraoperative visualization for resection of gliomas: the role of functional neuronavigation and intraoperative 1.5 T MRI," *Neurological Research*, vol. 28, no. 5, pp. 482–487, 2006.

[7] D. Lindner, C. Trantakis, C. Renner, et al., "Application of intraoperative 3D ultrasound during navigated tumor resection," *Minimally Invasive Neurosurgery*, vol. 49, no. 4, pp. 197–202, 2006.

[8] V. X. D. Yang, P. J. Muller, P. Herman, and B. C. Wilson, "A multispectral fluorescence imaging system: design and initial clinical tests in intra-operative photofrin-photodynamic therapy of brain tumors," *Lasers in Surgery and Medicine*, vol. 32, no. 3, pp. 224–232, 2003.

[9] R. Tréhin, J.-L. Figueiredo, M. J. Pittet, R. Weissleder, L. Josephson, and U. Mahmood, "Fluorescent nanoparticle uptake for brain tumor visualization," *Neoplasia*, vol. 8, no. 4, pp. 302–311, 2006.

[10] H. Stepp, T. Beck, T. Pongratz, et al., "ALA and malignant glioma: fluorescence-guided resection and photodynamic treatment," *Journal of Environmental Pathology, Toxicology and Oncology*, vol. 26, no. 2, pp. 157–164, 2007.

[11] M. A. Kara, F. P. Peters, F. J. W. ten Kate, S. J. van Deventer, P. Fockens, and J. J. G. H. M. Bergman, "Endoscopic video autofluorescence imaging may improve the detection of early neoplasia in patients with Barrett's esophagus," *Gastrointestinal Endoscopy*, vol. 61, no. 6, pp. 679–685, 2005.

[12] S. Andersson-Engels, C. Klinteberg, K. Svanberg, and S. Svanberg, "In vivo fluorescence imaging for tissue diagnostics," *Physics in Medicine and Biology*, vol. 42, no. 5, pp. 815–824, 1997.

[13] M. L. Harries, S. Lam, C. MacAulay, J. Qu, and B. Palcic, "Diagnostic imaging of the larynx: autofluorescence of laryngeal tumours using the helium-cadmium laser," *The Journal of Laryngology & Otology*, vol. 109, no. 2, pp. 108–110, 1995.

[14] W. Alian, S. Andersson-Engels, K. Svanberg, and S. Svanberg, "Laser-induced fluorescence studies of meso-tetra(hydroxyphenyl)chlorin in malignant and normal tissues in rats," *British Journal of Cancer*, vol. 70, no. 5, pp. 880–885, 1994.

[15] J. Blais, C. Amirand, J. P. Ballini, P. Debey, M. T. Foultier, and T. Patrice, "Photofrin-induced fluorescence in progressive and regressive murine colonic cancer cells: correlation with cell photosensitivity," *Journal of Photochemistry and Photobiology B*, vol. 27, no. 3, pp. 225–231, 1995.

[16] T. S. Mang, C. McGinnis, C. Liebow, U. O. Nseyo, D. H. Crean, and T. J. Dougherty, "Fluorescence detection of tumors: early diagnosis of microscopic lesions in preclinical studies," *Cancer*, vol. 71, no. 1, pp. 269–276, 1993.

[17] J. Shinoda, H. Yano, S.-I. Yoshimura, et al., "Fluorescence-guided resection of glioblastoma multiforme by using high-dose fluorescein sodium. Technical note," *Journal of Neurosurgery*, vol. 99, no. 3, pp. 597–603, 2003.

[18] W. Stummer, S. Stocker, S. Wagner, et al., "Intraoperative detection of malignant gliomas by 5-aminolevulinic acid-induced porphyrin fluorescence," *Neurosurgery*, vol. 42, no. 3, pp. 518–526, 1998.

[19] K. M. Hebeda, J. G. Wolbers, H. J. C. M. Sterenborg, W. Kamphorst, M. J. C. van Gemert, and H. A. M. van Alphen, "Fluorescence localization in tumour and normal brain after intratumoral injection of haematoporphyrin derivative into rat brain tumour," *Journal of Photochemistry and Photobiology B*, vol. 27, no. 1, pp. 85–92, 1995.

[20] A. Bogaards, A. Varma, K. Zhang, et al., "Fluorescence image-guided brain tumour resection with adjuvant metronomic photodynamic therapy: pre-clinical model and technology development," *Photochemical & Photobiological Sciences*, vol. 4, no. 5, pp. 438–442, 2005.

[21] A. Bogaards, A. Varma, S. P. Collens, et al., "Increased brain tumor resection using fluorescence image guidance in

a preclinical model," *Lasers in Surgery and Medicine*, vol. 35, no. 3, pp. 181–190, 2004.

[22] W. Stummer, A. Novotny, H. Stepp, C. Goetz, K. Bise, and H. J. Reulen, "Fluorescence-guided resection of glioblastoma multiforme by using 5-aminolevulinic acid-induced porphyrins: a prospective study in 52 consecutive patients," *Journal of Neurosurgery*, vol. 93, no. 6, pp. 1003–1013, 2000.

[23] V. Ntziachristos, C. Bremer, and R. Weissleder, "Fluorescence imaging with near-infrared light: new technological advances that enable in vivo molecular imaging," *European Radiology*, vol. 13, no. 1, pp. 195–208, 2003.

[24] B. W. Pogue, S. L. Gibbs, B. Chen, and M. Savellano, "Fluorescence imaging in vivo: raster scanned point-source imaging provides more accurate quantification than broad beam geometries," *Technology in Cancer Research & Treatment*, vol. 3, no. 1, pp. 15–21, 2004.

[25] V. Ntziachristos, E. A. Schellenberger, J. Ripoll, et al., "Visualization of antitumor treatment by means of fluorescence molecular tomography with an annexin V-Cy5.5 conjugate," *Proceedings of the National Academy of Sciences of the United States of America*, vol. 101, no. 33, pp. 12294–12299, 2004.

[26] E. E. Graves, D. Yessayan, G. Turner, R. Weissleder, and V. Ntziachristos, "Validation of in vivo flurochrome concentrations measured using fluorescence molecular tomography," *Journal of Biomedical Optics*, vol. 10, no. 4, Article ID 044019, 10 pages, 2005.

[27] S. V. Patwardhan, S. Bloch, S. Achilefu, and J. P. Culver, "Quantitative small animal fluorescence tomography using an ultrafast gated image intensifier," in *Proceedings of the 28th Annual International Conference of the IEEE Engineering in Medecine and Biology Society (EMBS '06)*, vol. 1, pp. 2675–2678, New York City, NY, USA, August-September 2006.

[28] D. Hall, G. Ma, F. Lesage, and Y. Wang, "Simple time-domain optical method for estimating the depth and concentration of a fluorescent inclusion in a turbid medium," *Optics Letters*, vol. 29, no. 19, pp. 2258–2260, 2004.

[29] K. R. Diamond, M. S. Patterson, and T. J. Farrell, "Quantification of fluorophore concentration in tissue-simulating media by fluorescence measurements with a single optical fiber," *Applied Optics*, vol. 42, no. 13, pp. 2436–2442, 2003.

[30] B. W. Pogue and G. Burke, "Fiber-optic bundle design for quantitative fluorescence measurement from tissue," *Applied Optics*, vol. 37, no. 31, pp. 7429–7436, 1998.

[31] J. R. Mansfield, K. W. Gossage, C. C. Hoyt, and R. M. Levenson, "Autofluorescence removal, multiplexing, and automated analysis methods for in-vivo fluorescence imaging," *Journal of Biomedical Optics*, vol. 10, no. 4, Article ID 041207, 9 pages, 2005.

[32] J. C. Finlay and T. H. Foster, "Recovery of hemoglobin oxygen saturation and intrinsic fluorescence with a forward-adjoint model," *Applied Optics*, vol. 44, no. 10, pp. 1917–1933, 2005.

[33] A. E. Profio, O. J. Balchum, and F. Carstens, "Digital background subtraction for fluorescence imaging," *Medical Physics*, vol. 13, no. 5, pp. 717–721, 1986.

[34] R. Weersink, M. S. Patterson, K. Diamond, S. Silver, and N. Padgett, "Noninvasive measurement of fluorophore concentration in turbid media with a simple fluorescence/reflectance ratio technique," *Applied Optics*, vol. 40, no. 34, pp. 6389–6395, 2001.

[35] H. J. C. M. Sterenborg, A. E. Saarnak, R. Frank, and M. Motamedi, "Evaluation of spectral correction techniques for fluorescence measurements on pigmented lesions in vivo," *Journal of Photochemistry and Photobiology B*, vol. 35, no. 3, pp. 159–165, 1996.

[36] R. S. Bradley and M. S. Thorniley, "A review of attenuation correction techniques for tissue fluorescence," *Journal of the Royal Society Interface*, vol. 3, no. 6, pp. 1–13, 2006.

[37] A. Bogaards, H. J. C. M. Sterenborg, and B. C. Wilson, "In vivo quantification of fluorescent molecular markers in real-time: a review to evaluate the performance of five existing methods," *Photodiagnosis and Photodynamic Therapy*, vol. 4, no. 3, pp. 170–178, 2007.

[38] M. Sinaasappel and H. J. C. M. Sterenborg, "Quantification of the hematoporphyrin derivative by fluorescence measurement using dual-wavelength excitation and dual-wavelength detection," *Applied Optics*, vol. 32, no. 4, pp. 541–548, 1993.

[39] R. Baumgartner and E. Unsöld, "High contrast fluorescence imaging using two-wavelength laser excitation and image processing," *Journal of Photochemistry and Photobiology B*, vol. 1, no. 1, pp. 130–132, 1987.

[40] H. J. C. M. Sterenborg, A. E. Saarnak, R. Frank, and M. Motamedi, "Evaluation of spectral correction techniques for fluorescence measurements on pigmented lesions in vivo," *Journal of Photochemistry and Photobiology B*, vol. 35, no. 3, pp. 159–165, 1996.

[41] A. Bogaards, H. J. C. M. Sterenborg, J. Trachtenberg, B. C. Wilson, and L. Lilge, "In vivo quantification of fluorescent molecular markers in real-time by ratio imaging for diagnostic screening and image-guided surgery," *Lasers in Surgery and Medicine*, vol. 39, no. 7, pp. 605–613, 2007.

[42] M. Roy and B. C. Wilson, "An accurate homogenized tissue phantom for broad spectrum autofluorescence studies: a tool for optimizing quantum dot-based contrast agents," in *Design and Performance Validation of Phantoms Used in Conjunction with Optical Measurements of Tissue*, vol. 6870 of *Proceedings of SPIE*, pp. 1–12, San Jose, Calif, USA, January 2008.

[43] W. Stummer, H. Stepp, G. Möller, A. Ehrhardt, M. Leonhard, and H. J. Reulen, "Technical principles for protoporphyrin-IX-fluorescence guided microsurgical resection of malignant glioma tissue," *Acta Neurochirurgica*, vol. 140, no. 10, pp. 995–1000, 1998.

[44] S. Lam, J. Hung, and B. Palcic, "Mechanism of detection of early lung cancer by ratio fluorometry," *Lasers in the Life Sciences*, vol. 4, no. 2, pp. 67–73, 1991.

[45] F. Duffner, R. Ritz, D. Freudenstein, M. Weller, K. Dietz, and J. Wessels, "Specific intensity imaging for glioblastoma and neural cell cultures with 5-aminolevulinic acid-derived protoporphyrin IX," *Journal of Neuro-Oncology*, vol. 71, no. 2, pp. 107–111, 2005.

[46] H. Heyerdahl, I. Wang, D. L. Liu, et al., "Pharmacokinetic studies on 5-aminolevulinic acid-induced protoporphyrin IX accumulation in tumours and normal tissues," *Cancer Letters*, vol. 112, no. 2, pp. 225–231, 1997.

[47] A. Orenstein, G. Kostenich, and Z. Malik, "The kinetics of protoporphyrin fluorescence during ALA-PDT in human malignant skin tumors," *Cancer Letters*, vol. 120, no. 2, pp. 229–234, 1997.

[48] L. Lilge and B. C. Wilson, "Photodynamic therapy of intracranial tissues: a preclinical comparative study of four different photosensitizers," *Journal of Clinical Laser Medicine and Surgery*, vol. 16, no. 2, pp. 81–91, 1998.

[49] E. H. Moriyama, S. K. Bisland, L. Lilge, and B. C. Wilson, "Bioluminescence imaging of the response of rat gliosarcoma to ALA-PpIX-mediated photodynamic therapy," *Photochemistry and Photobiology*, vol. 80, no. 2, pp. 242–249, 2004.

[50] P. J. Muller and B. C. Wilson, "Photodynamic therapy of brain tumors—a work in progress," *Lasers in Surgery and Medicine*, vol. 38, no. 5, pp. 384–389, 2006.

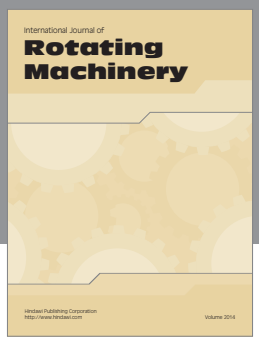

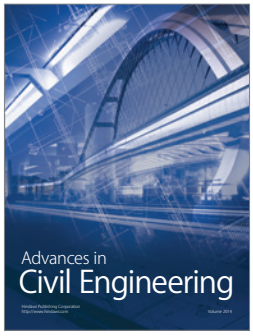

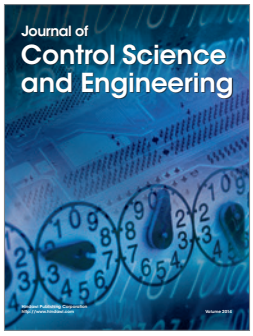

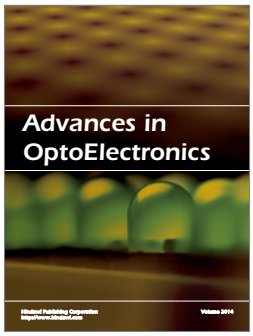

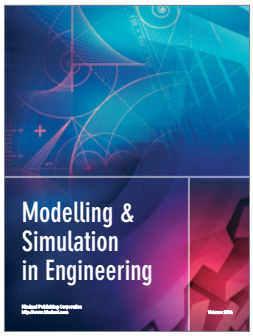

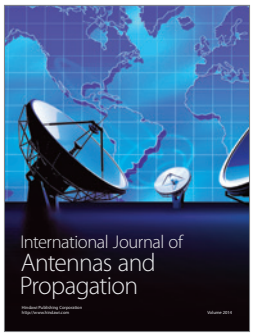

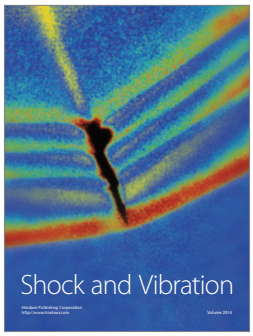

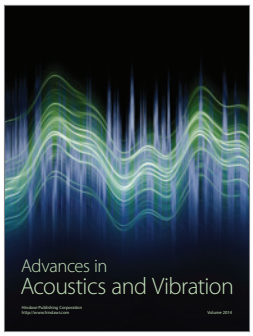

Hindawi

Submit your manuscripts at
http://www.hindawi.com